International Journal of Science and Research (IJSR)
ISSN: 2319-7064
SJIF (2020): 7.803

Design, Assembly and Geometric Characterization of Linear Paul Trap using Solidworks, Microscope, and Collimated Laser Beam

Naleli Jubert Matjelo[1], Ncamiso Khanyile[1]

[1]Stellenbosch University, Physics Department, Laser Research Institute, Stellenbosch, South Africa

Abstract: ***In this paper, the schematics of a linear Paul trap, designed using Solid works are presented. A careful procedure followed during electrode alignment, under the microscope, is discussed in detail. The assembled linear Paul trap is then characterized using a collimated 369 nm laser beam and the results are presented, analyzed, and discussed. The trap geometric parameters found in this work help guide the trap compensation with static potentials and characterization of the stability diagram of the ion trap.***

Keywords: Linear Paul Trap, Electrode Alignment, Microscope, Laser Beam, Characterization, Solid works

1. Introduction

The earliest ion traps were developed in the 1950s and1960s by Wolfgang Paul [1] and Hans Dehmelt [2]. Over time, ion traps proved to be very useful tools for studying various physical systems including quantum information processors [3], [4], [5], quantum simulators [6], [7], ion cavity QED [8], [9], frequency standards [10], [11]. There are different designs of ion traps, each of which is suited for some particular purpose. For instance, chip or microfabricated ion traps [12], [13] are well-suited for quantum information processing which require large arrays of traps to scale up information capacity. In some designs, the ion trap is placed in an optical cavity and this boosts the fidelity and speed of the trapped ion qubit measurement through the Purcell effect [14], [15]. There are approaches for ion trap designs with enhanced optical access including traps with one ring electrode or two opposing endcap electrodes or even planar trap geometries. The authors in [16] present a design of anion trap combined with a reflective parabolic surface with trap electrodes, thus, enhancing the efficiency of fluorescence collection. This parabolic trap design covers a solid angle of 2π steradians and allows precise ion placement at the focal point of the parabola [16].

a) Earnshaw's Theorem

According to Earnshaw's theorem it is impossible to trap ions in a stable spatial equilibrium using only static electric fields, so either a combination of electric and magnetic fields could be used (i .e. Penning traps) or a time-varying electric field could be used (i.e. Paul traps) [17]. This can be illustrated with an example of a charged particle supposedly trapped in a three dimensional harmonic electric potential of the following form [18],

$$\phi(x, y, z) = \alpha x^2 + \beta y^2 + \gamma z^2 \qquad (1)$$

According to Maxwell's equation the divergence of electric field (i.e.$\mathbf{E}(x, y, z) = \nabla\phi(x, y, z)$) in the absence of charge vanishes, that is,

$$\nabla . \boldsymbol{E}(x, y, z) = \Delta\phi(x, y, z) = 2(\alpha + \beta + \gamma) = 0 \quad (2)$$

This divergence implies that one of the components of the field has to be non-confining whenever the other two are confining. To prevent a charged particle from escaping along the non-confining field direction, the fields must be switched back and forth to alternate between confinement and non-confinement thus, resulting in trapping with electrodynamic fields.

b) Linear Paul Trap

A schematic of a linear Paul trap is shown in Figure 1 below with axes and electrodes labeled.

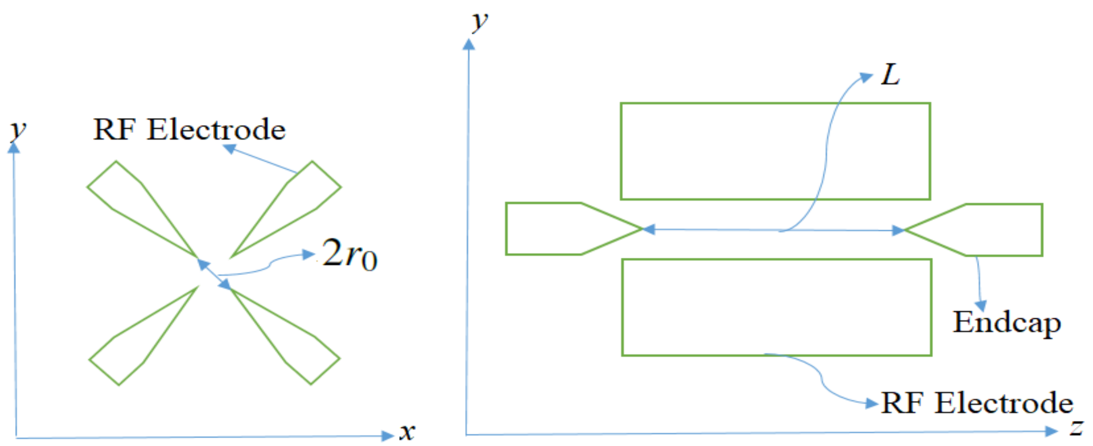

Figure 1: A schematic diagram of a linear Paul trap's cross-sectional view (left) and lateral view (right)

In the schematic diagram above, the xy-plane is also referred to as the radial plane while the z-axis is referred to as the trap axis. Compensation electrodes used for biasing the trap are not shown in this schematic diagram. When powered up with appropriate potential sources, a linear Paul trap produces a harmonic electric potential with static and time-varying components as shown below [18],

$$\phi(x,y,z,t) = \phi_{RF}(x,y,z,t) + \phi_{EC}(x,y,z) \quad (3)$$

with $\phi_{RF}(x,y,z,t)$ and $\phi_{EC}(x,y,z)$ being,

$$\phi_{RF}(x,y,z,t) = \frac{V_{RF}(x^2-y^2)}{2r_0^2}\cos(\Omega t) \quad (4)$$

$$\phi_{EC}(x,y,z) = \frac{V_{EC}}{L^2}(2z^2 - x^2 - y^2) \quad (5)$$

c) Trapped Ion Dynamics

The resulting Matthieu equations below govern the motion of a trapped ion [18],

$$\frac{d^2x}{d\tau^2} = -(a - 2q\cos(2\tau))x \quad (6)$$

$$\frac{d^2y}{d\tau^2} = -(a + 2q\cos(2\tau))y \quad (7)$$

$$\frac{d^2z}{d\tau^2} = -2az \quad (8)$$

with

$$\tau = \frac{1}{2}\Omega t \quad (9)$$

$$a = \frac{e\kappa V_{EC}}{mL^2\Omega^2} \quad (10)$$

$$q = \frac{2eV_{RF}}{mr_0^2\Omega^2} \quad (11)$$

Where Ω and V_{RF} are the angular frequency and amplitude of the radio frequency drive respectively, e and m are the charge and mass of the trapped particle respectively, V_{EC} is the static endcap potential, L is endcap to endcap spacing and $2r_0$ define the spacing between two diagonal RF electrodes. A dimensionless factor κ accounts for geometrical imperfections of the endcaps, which lead to experimental deviations from the pure quadrupole field [18]. The electric potential inside the trap resembles a saddle rotating at the RF drive frequency Ω.

The solution of the axial component of the equation of motion is simply a harmonic oscillator with axial trap frequency ω_z. On the other hand, the radial components lead to a solution that has two modes of oscillation; one at the trap/secular frequency ω_r while the other, called micromotion, is at the RF drive frequency. The trap frequencies are given by [18], [19],

$$\omega_z = \frac{\Omega}{2}\sqrt{2a} \quad (12)$$

$$\omega_r = \frac{\Omega}{2}\sqrt{\frac{q^2}{2} - a} \quad (13)$$

d) Trap Stability

The stability of Matthieu equations shown in the previous sections is determined by the values of a and q. The stability regions can also be shown graphically as shown in Figure 2below [19], [20].

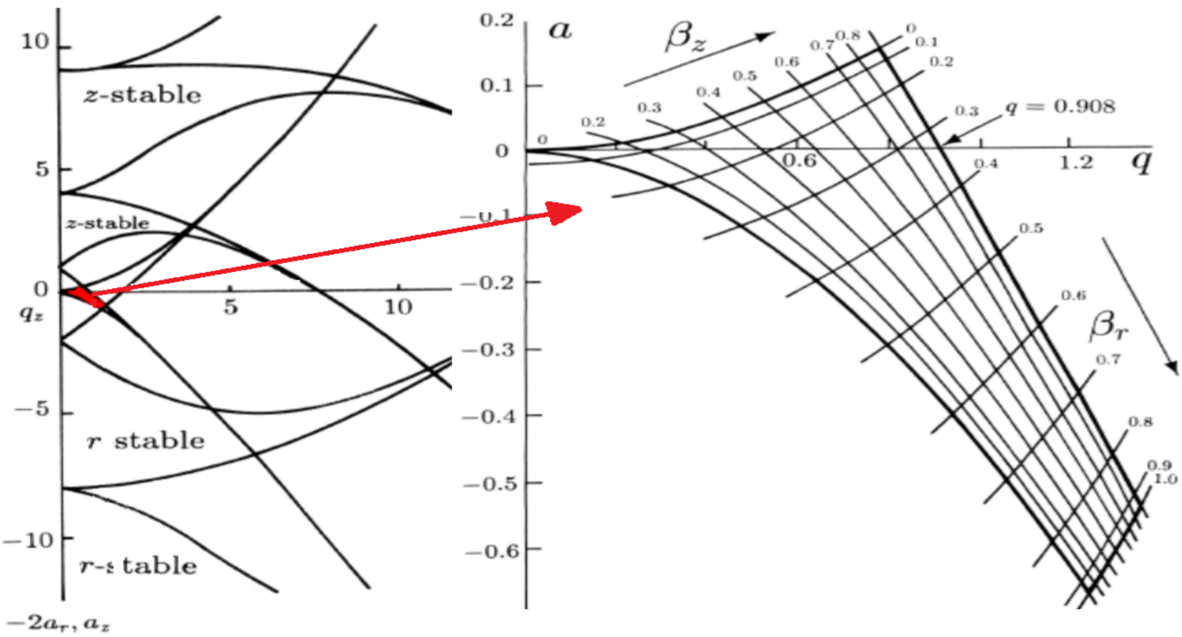

Figure 2: Stability map of a linear Paul ion trap [19].

The overlapping regions in the stability map are regions where the stability is achieved both axially, z and radially, r[19], [20]. The a and q parameters can be varied conveniently by changing the trap frequency or RF and DC voltages applied to the trap electrodes. This tuning of ion trap parameters is essential when relaxing and tightening the trap strength during the experiments. Linear Paul traps are typically operated with a q value below unity to keep excess micromotion reasonably small [18].

e) An Outline

The rest of this paper is organized as follows. Section II discusses the design of the linear Paul trap under Solid works environment, as well as the assembly and electrode alignment of the trap. Section III covers the measurements and characterization of the trap geometry using a collimated $369\ nm$ laser beam. Section IV presents the mounting and wiring of the trap. The ion trap testing is also carried out in this section with ions presented here as an indication of successful trapping of Ytterbium ion. Section V concludes this paper with a summary report of a few important findings in this work.

2. Trap Design and Implementation

a) Design Under CAD Environment

Figure 3 below shows a side view of a linear Paul trap design in a CAD environment.

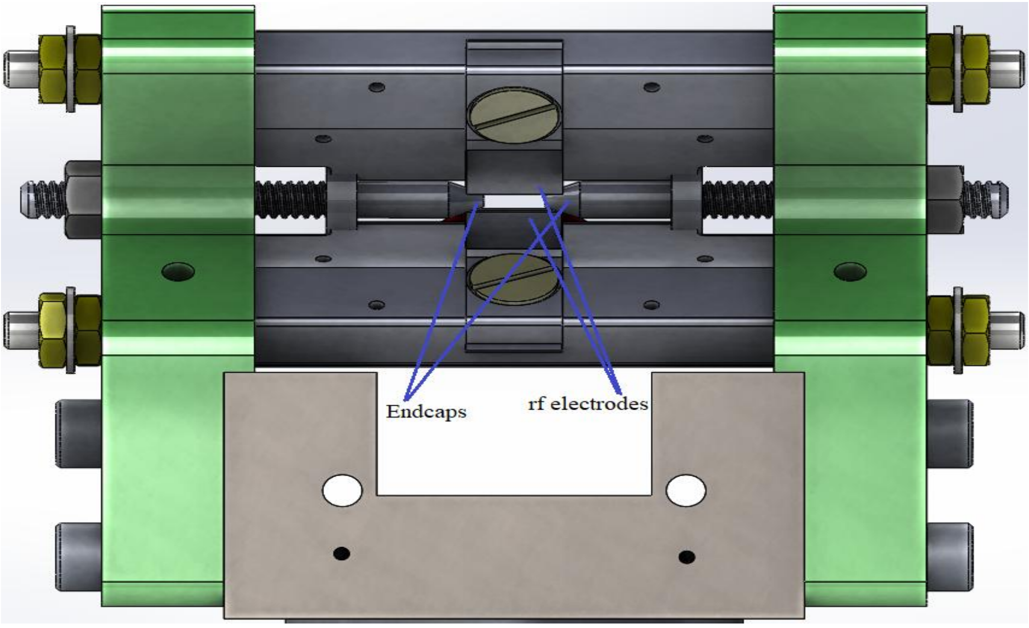

Figure 3: A picture of the side view of our trap design in CAD environment

Figure 4 below shows a cross-sectional view of a linear Paul trap design in a CAD environment.

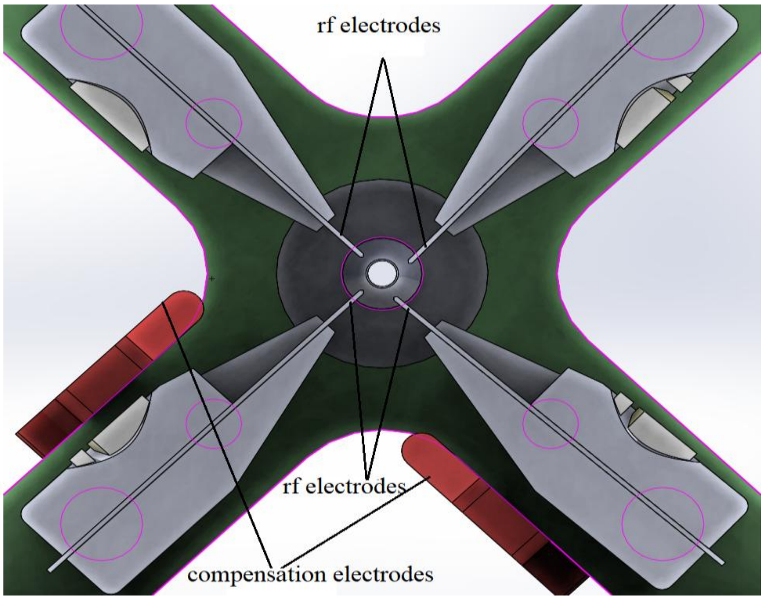

Figure 4: A picture of a cross-sectional view of a linear Paul trap design in CAD environment

There were no specific values of stability parameters (a and q) aimed for during the design of our design. This is primarily because we needed to be able to vary these stability parameters during experiments such that we can investigate different trapping points (stable and unstable) on the stability map. The choice was made to set the design parameters as follows;

- Diagonal RF electrode separation: $2r_0 = 1$ mm.
- Trap's axial length (endcap to endcap): $L = 5$ mm.
- RF drive frequency range: 15 MHz $\leq \frac{\Omega}{2\pi} \leq 20$ MHz.
- Leave V_{EC} and V_{RF} to vary as much as possible.
- Ytterbium had been chosen as the atom to create ions from, thus the charge to mass ratio $\frac{e}{m}$was already pre-decided.

With this set of choices, it is clear that stability parameters (a and q) will be adjusted using the tunable voltages V_{EC} and V_{RF} respectively. One limitation in the choice of trap dimensions was that for the same stability point at a chosen operating frequency, a large trap would require high voltages and that is expensive. The other limitation in our case was that a smaller trap would be tedious to align properly during assembly as we did all that manually under the microscope. The next section covers the alignment of electrodes.

b) Electrode Alignment Under Microscope

Our trap bears similarities to that used in the group of Rainer Blatt and has good optical access with endcap electrodes designed to shield the exposed dielectric surfaces. It was constructed out of gold-coated, oxygen-free copper. In our version, the RF electrodes are $200\ \mu m$ thick copper sheets clamped to stronger support. Figure 5 shows the top view of trap electrodes seen under the microscope after being tweaked.

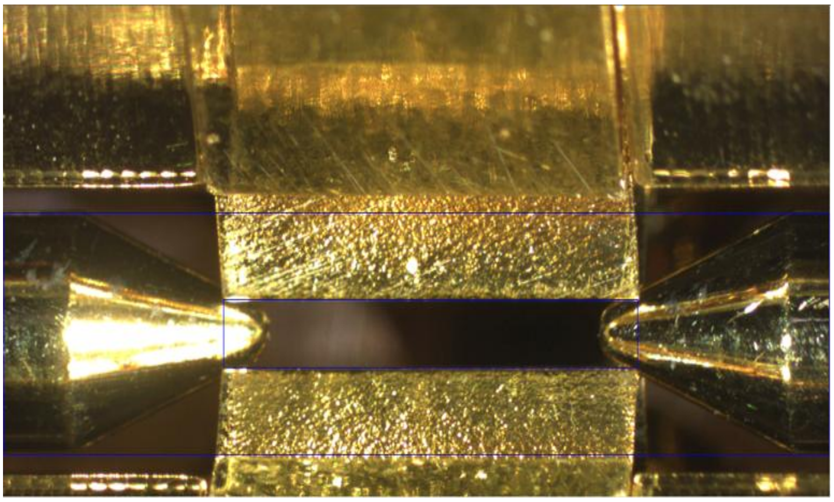

Figure 5: Top view of our linear Paul trap as seen under the microscope

The RF electrodes were positioned using a reference copper block which allowed only a prescribed length of the electrode to protrude out from its mounting platform. The electrodes were then tied down with bolts to secure them in their respective positions. The four RF electrode holders, endcaps, and the compensation electrodes were all assembled and held in place with stainless steel bolts on the ceramic frame and the base copper block to give a rigid structure. For finer adjustments of the RF and endcap electrodes orientation, the trap was placed under the microscope and tweaked with forceps while some bolts were slightly loosened and re-tightened when the electrode is in place. The blue rectangles are part of the tools (from the microscope software) which were useful in detecting and correcting the skewness of RF and endcap electrodes relative to one another. Figure 6 below shows the side view of the trap electrodes as seen under the microscope after tweaking.

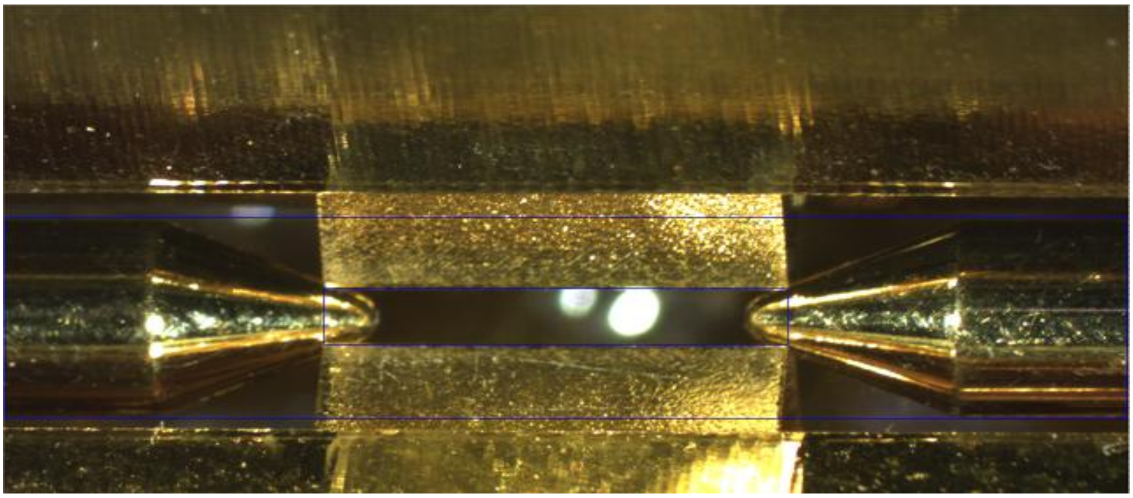

Figure 6: Side view of our linear Paul trap as seen under the microscope

A picture of our fully assembled linear Paul trap is shown in Figure 7 below. In this picture, the top compensation electrode can be seen, held down with bolts on the trap frame.

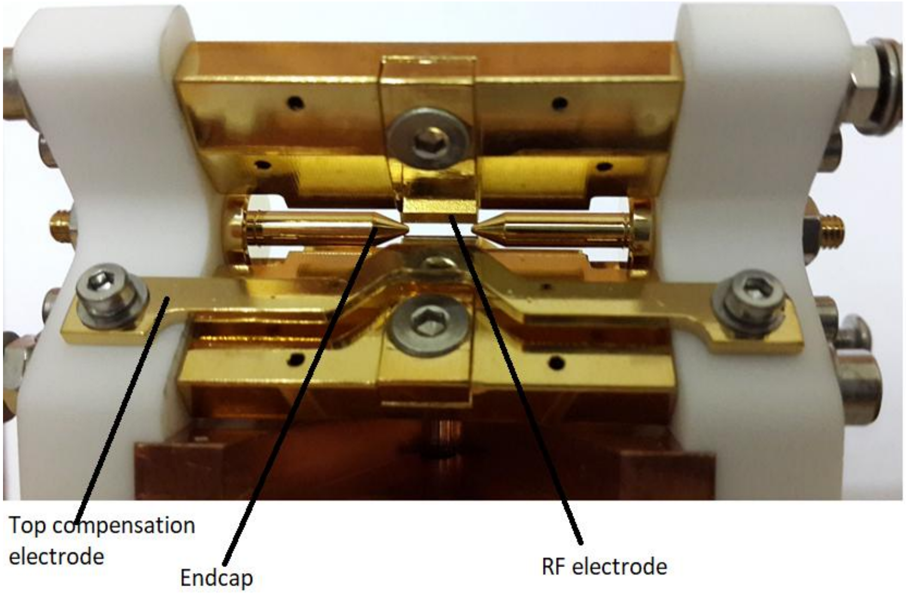

Figure 7: A picture of our actual linear Paul trap

The white support is made of ceramic and the copper block underneath the trap provides more structural rigidity to the entire setup.

3. Characterization Using Collimated Laser Beam

a) Trap Axis Length Measurements

After the tweaking process under the microscope, we mounted the whole trap setup on a translation stage and used the $369\ nm$ laser beam to measure the separation between endcaps and the separation between adjacent RF electrodes on two sides of the trap. We moved the trap on the translation stage horizontally and vertically, perpendicular to the laser beam direction, and recorded the micrometer reading upon reaching positions where half of maximum laser beam power passed through while the other half was blocked by the electrode. Following this procedure, the separation between the two endcaps was found to be $5.06\ mm$ as shown in Table 1 below.

Table 1: Laser coming from side 2 to side 1 of the trap. Trap sitting upright on the translation stage

Endcap 1	Endcap 2	Endcap Separation
17.212 mm	12.150 mm	5.062 mm

b) Measurements With Trap In Upright Position

Table 2 below shows the differences in the two endcap positions and the separation between RF electrodes as seen from the side with the trap sitting upright and laser beam going from side 2 to side 1 of the trap.

Table 2: The laser beam from side 2 to side 1 of the trap. Trap sitting upright on the translation stage

Laser Beam Position	Near Endcap 1	Near Endcap 2
Top RF electrode	22.974 mm	23.005 mm
Endcap Top Side	22.757 mm	22.832 mm
Endcap Bottom Side	22.316 mm	22.300 mm
Bottom RF electrode	22.142 mm	22.184 mm
RF electrode separation	0.832 mm	0.821 mm

From the measurement data in the table, a virtual line joining the two end caps is angled by no more than $0.334°$ to the assumed horizontal. This is an overestimation since the measurements from one end cap to the other were greater than $5.062\ mm$ but for estimating the deviation angles we used the separation of $5.062\ mm$ to set a loose upper bound. With respect to the same horizontal, the top and bottom RF electrodes are angled by no more than $0.351°$ and $0.476°$respectively. Hence the relative deviation between the two RF electrodes as seen from side 2 of the trap is no greater than $0.125°$. Table 3 below shows the differences in the two end cap positions and the separation between RF electrodes as seen from the side with the trap sitting upright and laser beam going from side 1 to side 2 of the trap.

Table 3: The laser beam from side 1 to side 2 of the trap. Trap sitting upright on the translation stage

Laser Beam Position	Near Endcap 1	Near Endcap 2
Top RF electrode	23.002 mm	22.983 mm
Endcap Top Side	22.922 mm	22.820 mm
Endcap Bottom Side	22.260 mm	22.315 mm
Bottom RF electrode	22.212 mm	22.205 mm
RF electrode separation	0.790 mm	0.778 mm

From the measurement data in the table, a virtual line joining the two endcaps is angled by no greater than $0.266°$ to the assumed horizontal. With respect to the same horizontal, the top and bottom RF electrodes are angled by no more than $0.216°$ and $0.080°$ respectively. Hence the relative deviation between the two RF electrodes as seen from side 1 of the trap is no greater than $0.137°$.

c) Measurements With Trap In Upright Position

Table IV below shows the differences in the two end cap positions and the separation between RF electrodes as seen from the top with the trap sitting on the side and laser beam going from top to bottom of the trap.

Table 4: The laser beam from side 2 to side 1 of the trap. Trap sitting upside-down on the translation stage.

Laser Beam Position	Near Endcap 1	Near Endcap 2
Top RF electrode	4.640 mm	4.641 mm
Endcap Top Side	4.520 mm	4.491 mm
Endcap Bottom Side	3.908 mm	3.975 mm
Bottom RF electrode	3.815 mm	3.851 mm
RF electrode separation	0.825 mm	0.790 mm

From the measurement data in the table, a virtual line joining the two end caps is angled by no greater than 0.216° to the assumed horizontal. With respect to the same horizontal, the top and bottom RF electrodes are angled by no more than 0.012° and 0.408° respectively. Hence the relative deviation between the two RF electrodes as seen from side 2 in an upside-down orientation of the trap is no greater than 0.397°. Table 5 below shows the differences in the two endcap positions and the separation between RF electrodes as seen from the bottom with the trap sitting on the side and laser beam going from bottom to top of the trap.

Table 5: The laser beam from side 1 to side 2 of the trap. Trap sitting upside-down on the translation stage

Laser Beam Position	Near Endcap 1	Near Endcap 2
Top RF electrode	5.055 mm	4.962 mm
Endcap Top Side	4.887 mm	4.760 mm
Endcap Bottom Side	4.371 mm	4.412 mm
Bottom RF electrode	4.205 mm	4.188 mm
RF electrode separation	0.850 mm	0.774 mm

From the measurement data in the table, a virtual line joining the two endcaps is angled by no greater than 0.487° to the assumed horizontal. With respect to the same horizontal, the top and bottom RF electrodes are angled by no more than 1.053° and 0.193° respectively. Hence the relative deviation between the two RF electrodes as seen from side 1 in an upside-down orientation of the trap is no greater than 0.861°.

d) Deductions From Measurements

Overall, the separation between RF electrodes near endcap 1and endcap 2 are $0.824\ mm \pm 0.044\ mm$ and $0.791\ mm \pm 0.037\ mm$ respectively. From these figures, we can infer that the separations between the diagonal RF electrodes near endcap1 and endcap 2 are greater than the aimed value of $2r_0 = 1\ mm$ by at most 17% and 12% respectively. The angular deviations of the RF electrodes from the trap axis are no more than 1.1°as viewed from both sides of the trap while sitting upright and upside-down. The relative angular deviation between adjacent RF electrodes is no more than 0.9° as viewed from both sides of the trap while sitting upright and upside-down.

4. Trap Wiring, Mounting, and Testing

a) Wiring and Mounting

After alignment of the ion trap electrodes, the trap was mounted and clamped with screws on the rails inside the vacuum chamber as shown in Figure 8 below.

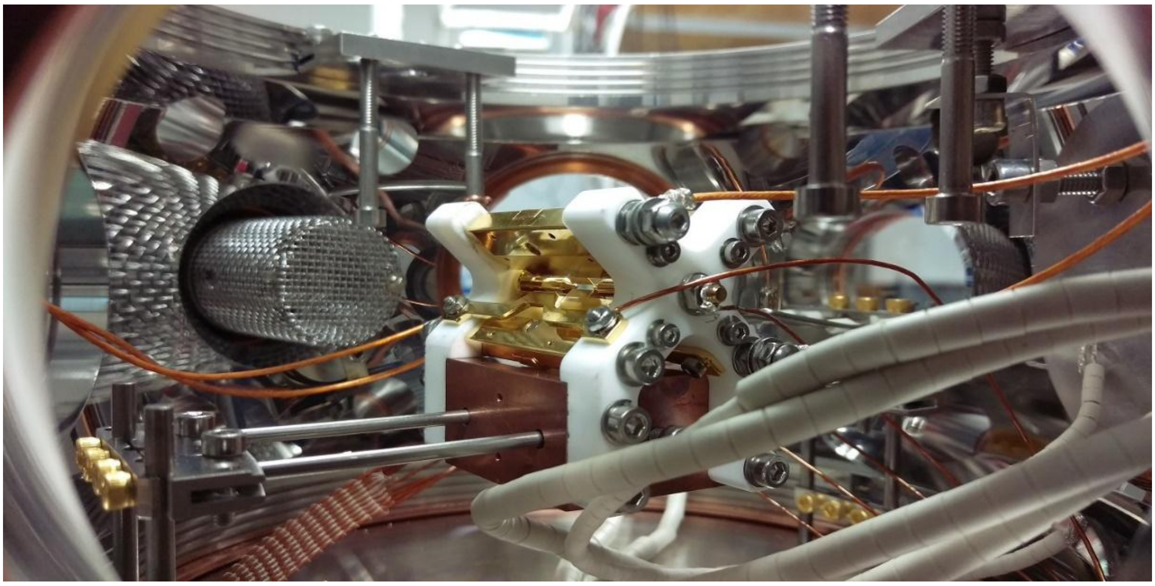

Figure 8: The ion trap inside the vacuum chamber with the wiring to all the electrodes

Steatite ceramic beads were used to provide insulation to the bare wires to reduce the chances of unwanted short circuits.

b) Ion Trapping Attempt

With all the necessary optics, RF sources, and vacuum systems in place the assembled ion trap was able to trap Ytterbium ions as Figure 9 below shows one of the many successful Ytterbiumion trapping (and crystallization) attempts.

Figure 9: A chain of trapped Ytterbium ions

The ions were imaged using a camera and a stack of lenses, which help capture the $369\ nm$ photons spontaneously emitted from the $^2S_{1/2}|F = 1\rangle \leftrightarrow {}^2P_{1/2}|F = 0\rangle$ transition of the trapped Ytterbium ions.

5. Conclusion

In this paper, we presented the overview of the Solid works-based design schematics for our linear Paul trap. The ion trap parts assembly and electrode alignment under the microscope followed this. The spacing between endcaps was found to be $5.06\ mm$ with an endcap-to-endcap angular deviation of no more than $0.4°$_as viewed from both sides of the trap, upright and upside-down. The separations between the RF electrodes near endcap 1 and endcap 2 were found to be$0.824\ mm \pm 0.044\ mm$ and $0.791\ mm \pm 0{:}037\ mm$ respectively. When viewed from both sides of the trap, both while sitting upright and upside-down, the angular deviations of the electrodes from the trap axis and the relative angular deviations between adjacent RF electrodes were found to be no more than $1{:}1°$ and $0.9°$ respectively. These findings were useful in guiding the next step of trap compensation through static potentials.

6. Acknowledgements

We would like to acknowledge Stellenbosch University and the Council for Scientific and Industrial Research for their financial assistance and provision of lab facilities to make this work a success.

References

[1] Paul, W. (1990). Electromagnetic traps for charged and neutral particles. Rev. Mod. Phys, 62: 531 - 540.

[2] Dehmelt, H.G. (1967).Radiofrequency spectroscopy of stored ions i: Storage. Adv. At. Mol. Phys, 3: 53.

[3] Cirac, J.I. and Zoller, P. (1995). Quantum computations with cold trapped ions. Phys. Rev. Lett., 74: 4091-4094.

[4] Wineland, D. J., Monroe, C., Itano, W.M., Leibfried, D., King, B.E.and Meekhof, D.M. (1998). Experimental issues in coherent quantum-state manipulation of trapped atomic ions. J. Res. Nat. Inst. Stand. Tech., 103: 259 - 328.

[5] Haffner, H., Roos, C.F. and Blatt, R. (2008). Quantum computing with trappedions. Phys. Rep., 469: 155 - 203.

[6] Friedenauer, A., Schmitz, H., Glueckert, J.T., Porras, D. and Schaetz, T. (2008).Simulating a quantum magnet with trapped ions. Nature Phys, 4: 757 - 761.

[7] Kim, K., Chang, M.S., Korenblit, S., Islam, R., Edwards, E.E., Freericks, J.K., Lin, G.D., Duan, L.M. and Monroe, C. (2010). Quantum simulation of frustrated Ising spins with trapped ions. Nature, 465: 590 - 593.

[8] Keller, M., Lange, B., Hayasaka, K., Lange, W. and Walther, H. (2003). Deterministic cavity quantum electrodynamics with trapped ions. J. Phys. B: At. Mol. Opt. Phys, 36: 613 - 622.

[9] Herskind, P.F., Dantan, A., Marler, J.P., Albert, M. and Drewsen M. (2009).Realization of collective strong coupling with ion Coulomb crystals inan optical cavity. Nature Phys, 5: 494 – 498.

[10] Webster, S.A., Taylor, P., Roberts, M., Barwood, G.P.and Gill, P. (2002). Kilohertz-resolution spectroscopy of the 2s1/2 - 2f7/2 electric octupole transition in a single 171 Yb+ ion. Phys. Rev. A, 65: 052501.

[11] Chwalla, M., Benhelm, J., Kim, K., Kirchmair, G., Monz, T., Riebe, M., Schindler, P., Villar, A.S., Hansel, W., Roos, C.F., Blatt, R., Abgrall, M., Santarelli, G., Rovera, G.D. and Laurent P. (2009). Absolute frequency measurement of the 40Ca+ 4s 2s1/2 - 3d 2d5/2 clock transition. Phys. Rev. Lett., 102: 023002.

[12] Hughes, M.D., Lekitsch, B., Broesma, J.A. and HesingerW. K. (2011). Microfabricated ion traps. arXiv: 1101.3207 [quant-ph].

[13] Amini, J.M., Britton, J., Leibfried, D. and Wineland, D.J. (2008). Microfabricated chip traps for ions. arXiv: 0812.3907v1 [quant-ph].

[14] Purcell, E. M. (1946). Spontaneous emission probabilities at radio frequencies. Phys. Rev. 69, 681, 1946.

[15] Milonni, P. W. (1993). The Quantum Vacuum: An Introduction to Quantum Electrodynamics. Academic Press.

[16] Chou, C., Auchter, C., Lilieholm, J., Smith, K. and Blinov, B. (2017). Singleion imaging and fluorescence collection with a parabolic mirror trap. Review of Scientific Instruments, 88: 086101.

[17] National Academies of Sciences Engineering and Medicine. Quantum Computing: Progress and Prospects. The National Academies Press, Washington, DC, 2019.

[18] Wieburg, P. (2014). A linear paul trap for ytterbium ions. Master's thesis, Universitat Hamburg.

[19] March, R. E. (1997). An introduction to quadrupole ion trap mass spectrometry. Journal of Mass Spectrometry, 32: 351 - 369.

[20] Leibfried, D., Blatt, R. Monroe, C. and Wineland, D. (2003). Quantum dynamics of single trapped ions. Reviews of Modern Physics, 75: 281 - 324.